Japanese Journal of Gastroenterology and Hepatology

Research Article

ISSN: 2435-1210 | Volume 9

Identification of Pyroptosis-Related Subtypes in Liver Cancer, Establishment of Prognostic Models, and Characterization of Tumor Microenvironment Infiltration

Chen Y[1], Zhou W[2], Gong Y[2], Wang H[2], Ma Y[2], Zhao L[2] and Ou X[2]

[1]Anhui Medical University, Peking University Shenzhen Hospital Clinical School, Futian District, Guangdong Province, China

[2]Peking University Shenzhen Hospital, Futian District, Shenzhen, Guangdong Province, China

***Corresponding author:**

Xi Ou,
Peking University Shenzhen Hospital, 1120 Lianhua Road, Futian District, Shenzhen, Guangdong, 518036, China, E-mail: bdszyyox@163.com

Received: 29 Jul 2022
Accepted: 08 Aug 2022
Published: 13 Aug 2022
J Short Name: JJGH

Citation:

Qu X. Identification of Pyroptosis-Related Subtypes in Liver Cancer, Establishment of Prognostic Models, and Characterization of Tumor Microenvironment Infiltration. J Gstro Hepato. V9(4): 1-14

1. Abstract

1.1. Objectives: Pyroptosis is a type of programmed cell death that has been discovered and confirmed in recent years, which were characterized by pro-inflammatory and is related to tumor progression, prognosis and treatment response. However, the potential roles of pyroptosis-related genes (PRGs) in the tumor microenvironment (TME) remain unclear. At the same time, in order to understand the underlying mechanisms of liver tumorigenesis and predict the response to immunotherapy, our study on the characteristics of multiple PRG-mediated TME cell infiltration may provide important ideas and directions for future research.

1.2. Methods: We characterized PRG changes in 115 liver cancer patient (HCC) samples from the genetic and transcriptional domains and assessed their expression patterns from the GEO dataset. Then, a prognostic model for predicting survival was constructed and its predictive ability in HCC patients was validated. Finally, we constructed a highly accurate nomogram to improve the clinical applicability of the prognostic model.

1.3. Results: A prognostic model was constructed and its accuracy was determined. Two distinct molecular subtypes were identified, and multilayered PRG alterations were found to correlate with the clinical features, prognosis, and TME cell infiltration characteristics of patients. The high-risk group had high levels of Macrophages M2 and low levels of T cells CD8. StromalScore, ImmuneScore, ESTIMATEScore scores were higher in the low-risk group. Risk scores of patients in the three subtypes of genotyping were positively correlated with tumor mutational burden.

1.4. Conclusions: Our comprehensive analysis of PRGs in HCC demonstrates their potential roles in tumor-immunity-tumor microenvironment, clinical features and prognosis. These findings may improve our understanding of PRGs in HCC and provide new directions and avenues for assessing prognosis and developing more effective immunotherapy strategies.

2. Foreword

Hepatocellular carcinoma is one of the most common malignant tumors with strong metastasis and poor prognosis. It is also one of the leading causes of cancer-related death, and its morbidity and mortality ranks sixth and fourth in the world, respectively. At present, the research on liver cancer mainly focuses on apoptosis, autophagy and angiogenesis [1, 2]. In recent years, with the in-depth research on the pathogenesis of liver cancer and the progress of precision medicine and modern molecular biotechnology, the role of pyroptosis in the occurrence, development and treatment of liver cancer has been gradually discovered. Pyroptosis is a pro-inflammatory programmed cell death method discovered and confirmed in recent years, which is different from any cell death method seen before. Rapid DNA fragmentation, cell membrane rupture, and production of proinflammatory cytokines are hallmarks of pyroptosis. In other words, pyroptosis has some morphological features of apoptosis and necrosis at the same time [3-5]. Pyroptosis is classified into Caspase-dependent. 1 of the classical pyroptotic pathway and Caspase-4/5/11-dependent non-classical pyroptotic pathway [6]. The production of activated Caspase-1 is the key to the process of pyroptosis. A study reported that 3 cases of liver cancer and its paired adjacent tissues were subjected to immunohistochemistry with Caspase-antibody, and the results showed that the expression of caspase-1 was low in liver cancer tissues [7]. Pyroptosis of liver non-parenchymal cells can lead to

severe inflammation and liver fibrosis, manifested by infiltration of neutrophils and collagen deposition caused by activated hepatic stellate cells [8]. Some studies have also found that in liver cancer tissues and liver cancer cell lines, hypoxia-induced high Caspase-1 activity and subsequent production of a variety of inflammatory factors can promote cancer cell invasion and metastasis [9]. It can be seen that pyroptosis can not only inhibit tumor cell proliferation, but also form a microenvironment that promotes tumor cell growth [10, 11].

More and more studies have shown that pyroptosis is involved in the remodeling of the Tumor Microenvironment (TME) [12]. Since pyroptosis is highly immunogenic, it induces local infiltration by attracting inflammatory cells followed by local inflammation, thereby alleviating immunosuppression and inducing an immune response in the TME [13]. At the same time, TME also has potential impact on the occurrence and development of cancer. Under normal conditions, the stroma maintains homeostasis and acts as a barrier to tumorigenesis. However, when cells become cancerous, the surrounding stroma also changes to support tumor progression [14, 15]. Of the published studies, most of them evaluate only one or a few Pyroptosis-Related Genes (PRGs) and cell types, yet the antitumor effect is due to numerous genes interacting in a highly coordinated manner. Therefore, to understand the underlying mechanisms of liver tumorigenesis and predict the response to immunotherapy, our study of the characteristics of multiple PRG-mediated TME cell infiltration may provide important ideas and directions for future research.

This study comprehensively assessed the expression profiles of PRGs and obtained an overview of immune infiltration within tumors using two computational algorithms; namely, CIBERSORT and ESTIMATE. First, 115 HCC patients were stratified into two discrete subtypes according to PRG expression levels. Patients were then divided into three genetic subtypes based on Differentially Expressed Genes (DEGs) identified based on the two pyroptotic subtypes. We further established a scoring system to predict patient survival and characterize the immune status of PLC, while screening some sensitive chemotherapeutic drugs to accurately predict patient prognosis and response to immunotherapy.

3. Materials and Methods

3.1. Data Sources

We downloaded the gene expression (fragments per kilobase, FPKM) and clinical relevance of liver cancer from The Cancer Genome Atlas Program (TCGA) database (https://portal.gdc.cancer.gov/) data. Download GEO data from Gene Expression Omnibus (GEO) (https://www.ncbi.nlm.nih.gov/geo/). A total of one GEO HCC cohort (GSE 76427) and TCGA cohort were obtained for subsequent analysis. We collated and ID-transformed the transcriptome data, as well as the clinical data. Meanwhile, the FPKM values of TCGA-HCC were converted into Transcripts Per Kilobase Million (TPM) using the limma package in R studio software [16]. Finally, a total of 115 HCC patients were included in the follow-up analysis, and clinical variables included age, gender, survival time, survival status, and TNM stage.

3.2. Consensus Cluster Analysis of PRGs

We retrieved 52 pyroptosis-related genes from previously published studies and the MSigDB team (REACTOME_PYROPTOSIS) (http://www.broad.mit.edu/gsea/msigdb/) [17, 18]. Consensus cluster typing was performed using the ConsensusClusterPlus package in R studio software, and patients were divided into different molecular subtypes according to the expression of pyroptotic cell genes. The criteria for typing are based on high correlations within subtypes and low correlations between subtypes after typing. At the same time, the subgroups after typing were compared by survival analysis. Finally, to investigate differences in PRGs in biological processes, a Gene Set Variation Analysis (GSVA) was performed using a marker gene set (c2.cp.kegg.v7.4.symbols) derived from the MSigDB database.

3.3. Clinical features and prognosis of liver cancer in different molecular subtypes

To examine the clinical value of the different subtypes identified by consensus clustering, we compared age, sex, and tumor stage between the different subtypes. GSVA analysis was also performed to explore pathways active in different subtypes. Survival differences between subtypes were assessed using Kaplan-Meier curves generated by the "survival" and "survminer" packages in the R studio software.

3.4. DEG identification and GO and KEGG enrichment analysis

DEGs between different pyroptotic subtypes were identified using the "limma" and "VennDiagram" packages in the R studio software. We set logFCfilter=0.585, and the adjusted P value is <0.05. To further explore the potential functions of differential genes in different typing and determine the enrichment of their functions and pathways, we performed GO and KEGG enrichment analysis of differential genes using the "clusterprofiler" and "enrichplot" packages in R studio software.

3.5. Constructing a Pyroptosis-Related Prognosis

We identified differential genes associated with prognosis using the 'limma' and 'survival' packages in R studio software. Then, the differential genotypes were genotyped and the survival time of different genotypes was analyzed. Finally, all HCC patients were randomly divided into a train group (n=243) and a test group (n=242) in a ratio of 1:1. Based on the prognostic genes associated with pyroptosis, the Lasso Cox regression algorithm was used in the R studio software. The "glmnet" R package minimizes the risk of overfitting. According to the median risk score, the train group and the test group were divided into low-risk (PRG_score < median) and high-risk (PRG_score > median) groups, and then survival difference analysis was performed and ROC curves were drawn.

3.6. Correlation and drug susceptibility analysis of molecular subtypes and TME in HCC

The levels of immune cells in different subtypes of HCC were determined using the single-sample gene set enrichment analysis (ssG-

SEA) algorithm. To explore whether there is a difference in the therapeutic effect of drugs in high- and low-risk groups, we calculated the half-inhibitory concentration (IC50) values of drugs commonly used in the treatment of HCC using the "pRRophetic" package in R studio software.

3.7. Building a Nomogram Scoring System

Predictive nomograms were developed using the "rms" package in R studio software with clinical characteristics and risk scores. In the nomogram scoring system, each variable is matched with a score, and the total score is obtained by adding the scores of all variables for each sample. Calibration plots of nomograms were used to describe predicted values between predicted 1-, 3-, and 5-year survival events and actual observed outcomes.

3.8. Statistical Analysis

All statistical analyses were performed using R version 4.1.2 and P less than 0.05 was considered statistically significant.

4. Result

4.1. Genetic and Transcriptional Alterations of PRGs in HCC

This study included 52 pyroptosis-related genes, and summarized and analyzed the incidence of somatic mutations in these 52 PRGs. Figure 1A shows that among 364 samples, 157 (43.13%) had mutations in PRG. Among them, TP53 had the highest mutation frequency of 30%, followed by NLRP2 (2%) and NLRP3 (2%). We found the following 30 PRGs (SCAF11, PJVK, GSDMA, GPX4, CASP9, CASP6, IL1A, GSDME, CYCS, CHMP4B, CHMP4A, CHMP3, CHMP2A, CASP5, CASP1, BAK1, GZMA, TNF, TIRAP, PYCARD, NOD1, NLRP1, IL6, AIM2, IRF1, IL1B, IL18, CHMP7, CHMP4C and CHMP2B) without any mutations. We continued to explore changes in cellular copy number in these PRGs, and Figure 1B shows the increase and loss of copy number variation frequency in PRGs. We found copy number changes in all 52 PRGs, among which

GSDMC, AIM2, GSDMD, CHMP6 all have increased copy number variation, while CASP9, HMGB1, IRF2, GASP3, GPX4 and TP53 all had reduced copy number variation. In Figure 1C, the location of CNV alterations in PRGs on their respective chromosomes is shown. In Figure 1D, we found that both copy number increased genes and copy number decreased genes were up-regulated in liver cancer samples, and most genes were differentially expressed in normal and tumor tissues. It can be seen that the link between copy number variation and liver cancer is not very strong, but PRGs generally have significant differences between normal and liver cancer tissues, indicating the potential impact of PRGs in liver tumor formation.

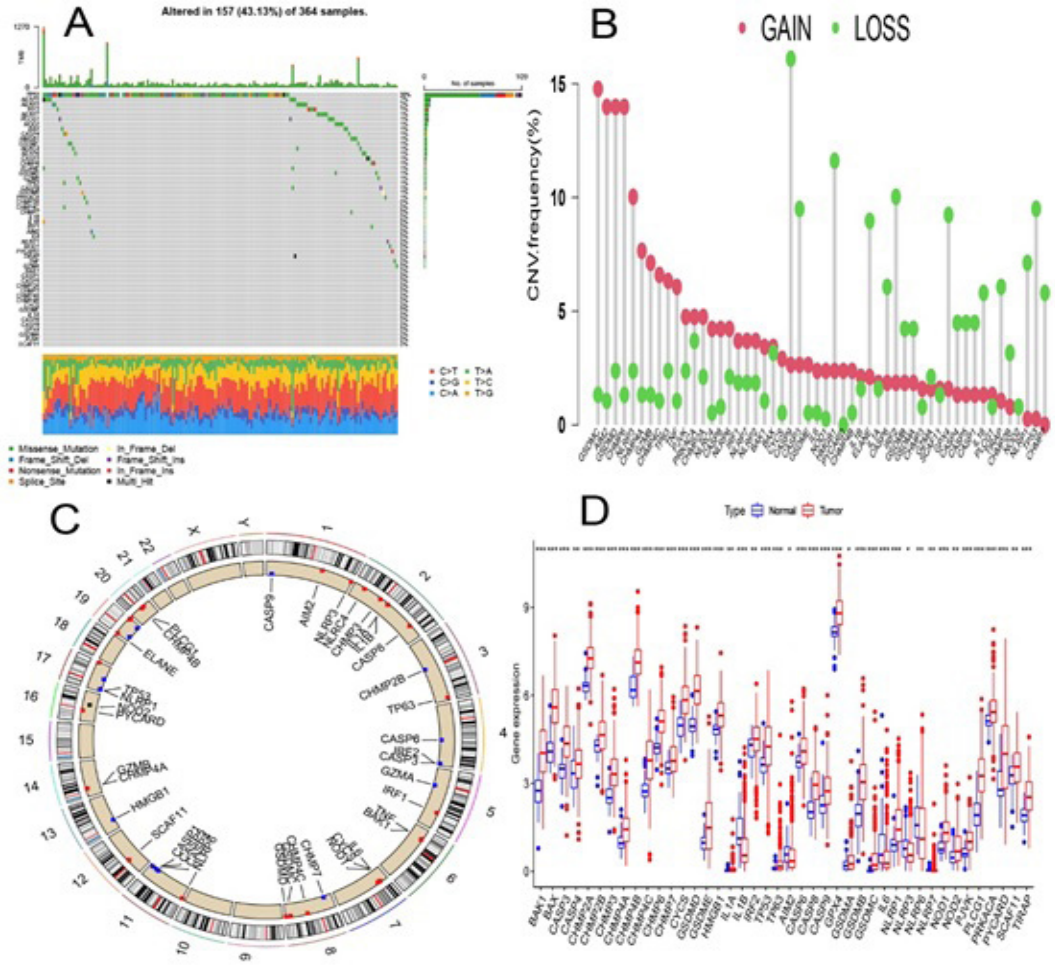

Figure 1: Genetic and transcriptional alterations of PRGs in HCC. (A) Mutation frequencies of 52 PRGs in 115 patients from the TCGA cohort. (B) Frequency of CNV gain and loss in PRG. (C) Location of CNV alterations in PRGs on 23 chromosomes. (D) Expression distribution of 52 PRGs between normal and HCC tissues. PRG, pyroptosis-related gene; HCC, liver cancer; TCGA, The Cancer Genome Atlas; CNV, copy number variant

4.2. Identification of Pyroptotic Subtypes in PLC

The HCC cohort (GSE76427) used in this study has a total of 115 patients, we used the "survival" and "limma" packages in R studio software to analyze the prognostic value of PRG in 115 HCC patients, P<0.05 was considered statistically significant significance. Figure 2A shows the co-expression relationship between genes, and it can be seen that GSDME, CHMP4B, CHMP3, BAK1 and NOD2 are high-risk genes strongly associated with prognosis. We also found that there is a negative correlation between NLRP6 and multiple genes, which may provide a certain direction for future research on the prognosis of liver cancer. To further study the expression characteristics of PRGs in HCC patients, we used the "ConsensusClusterPlus" package in R studio software to classify HCC patients according to the expression levels of 52 PRGs with a consensus clustering algorithm (Figure 2B). The results show that k=2 seems to be the best choice for classifying the whole cohort into A and B subtypes, and PCA analysis also shows that the samples of subtype A and subtype B can be divided according to the expression of pyroptosis-related genes (Figure 2C). In Figure 2D we then performed a survival analysis, unfortunately we found no significant difference in survival prognosis between subtype A and subtype B, but it can be seen that the survival rate of subtype A was higher than that of subtype B during the first 5 years. In addition, we revealed significant differences in PRG expression and clinical characteristics by comparing the clinical characteristics of the two subtypes of HCC. Figure 2E shows that most pyroptosis-related genes are generally high in subtype A by age, sex, and tumor status. state of expression.

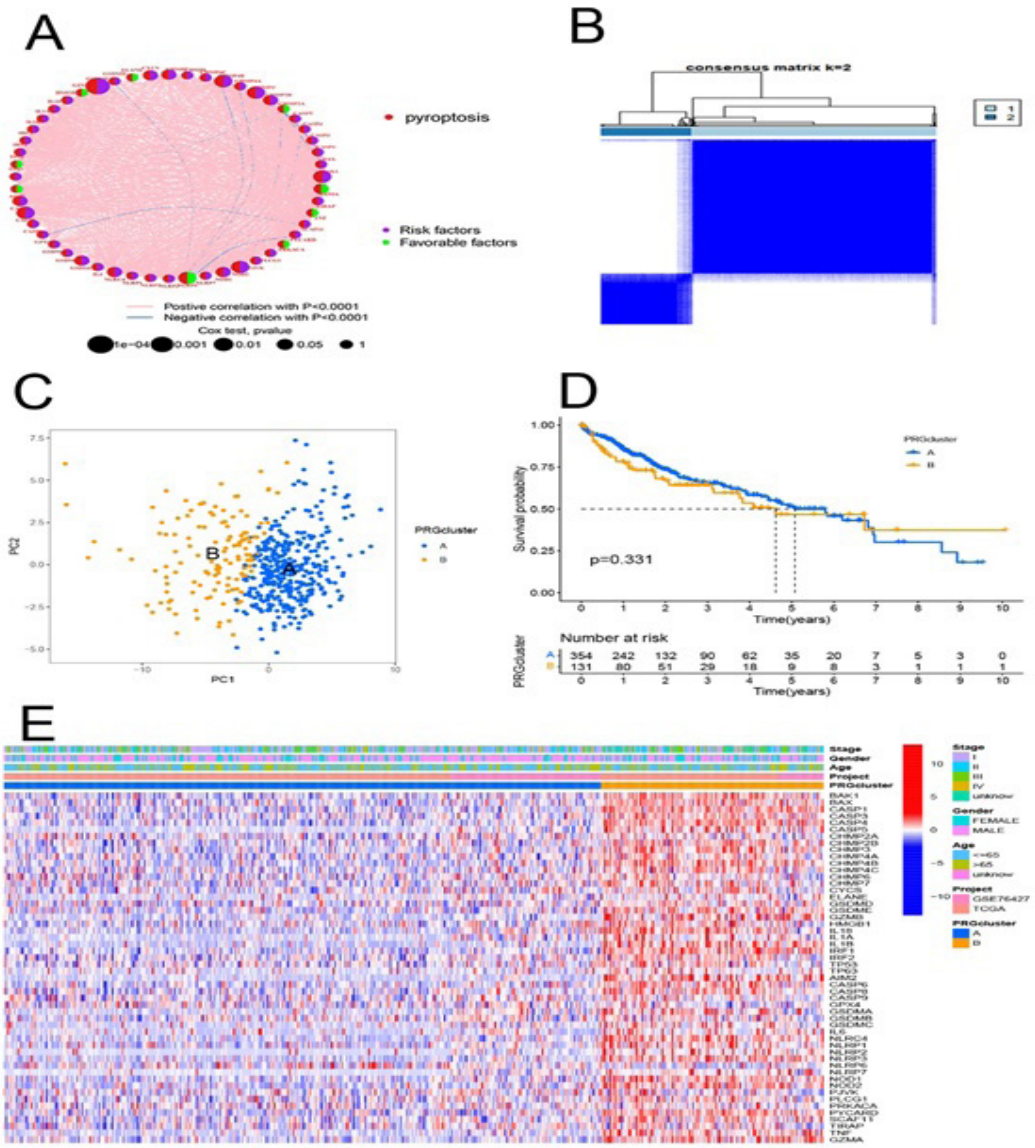

Figure 2: Clinical and biological characteristics of PRG subtypes and two different sample subtypes, divided by the same cluster. (A) Interactions between PRGs in HCC. The lines connecting the PRGs represent their interactions, and the thickness of the lines represents the strength of the association between the PRGs. Green and magenta represent negative and positive correlations, respectively. (B) Consensus matrix heatmap defining two clusters (k = 2) and their associated regions. (C) PCA analysis revealed significant differences in transcriptomes between the two isoforms. (D) Univariate analysis showing 52 PRGs associated with survival time. (E) Differences in clinical features and PRG expression levels between the two different subtypes. PRG, pyroptosis-related gene; HCC, liver cancer; PCA, principal component analysis

4.3. Characteristics of the tumor microenvironment in different subtypes

Figure 3A shows that we through enrichment analysis GSVA, A subtypes active path has the following MATURITY_ONSET_DIABETES_OF_THE_YOUNG, OLFACTORY_TRANSDUCTION, ARGININE_AND_PROLINE_METABOLISM, PEROXISOME, FATTY_ACID_METABOLISM, BUTANOATE_METABOLISM, GLYCINE_SERINE_AND_THREONINE_METABOLISM, PPAR_SIGNALING_PATHWAY, PRIMARY_BILE_ACID_BIOSYNTHESIS, RETINOL_METABOLISM, DRUG_METABOLISM_CYTOCHROME_P450, TYROSINE_METABOLISM HISTIDINE_METABOLISM. Active pathways in subtype B are NOD_LIKE_RECEPTOR_SIGNALING_PATHWAY, LEISHMANIA_INFECTION, FC_GAMMA_R_MEDIATED_PHAGOCYTOSIS, T_CELL_RECEPTOR_SIGNALING_PATHWAY, B_CELL_RECEPTOR_SIGNALING_PATHWAY, PATHOGENIC_ESCHERICHIA_COLI_INFECTION KEGG_ENDOCYTOSIS. To further investigate the role of PRG in HCC patients, we evaluated the correlation between the two subtypes and 23 human immune cell subsets in each HCC sample, as can be seen in Figure 3B, the two subtypes were mostly associated with immune cells Significant differences exist in the presence of infiltration. The invasiveness of Eosinophilna in subtype A was significantly higher than that in subtype B, while in Activated.B.cellna, Activated.CD4.T.cellna, Activated.CD8.T.cellna, Activated.dendritic.cellna, Gamma.delta.T .cellna, Immature..B.cellna, Immature.dendritic.cellna, MDSCna Macrophagena, Mast.cellna, Natural.killer.T.cellna, Natural.killer.cellna, lasmacytoid.dendritic.cellna, Regulatory.T.cellna, T Among .follicular.helper.cellna, Type.1.T.helper.cellna, Type.17.T.helper.cellna Type.2.T.helper.cellna, the B subtype was significantly higher than the A subtype.

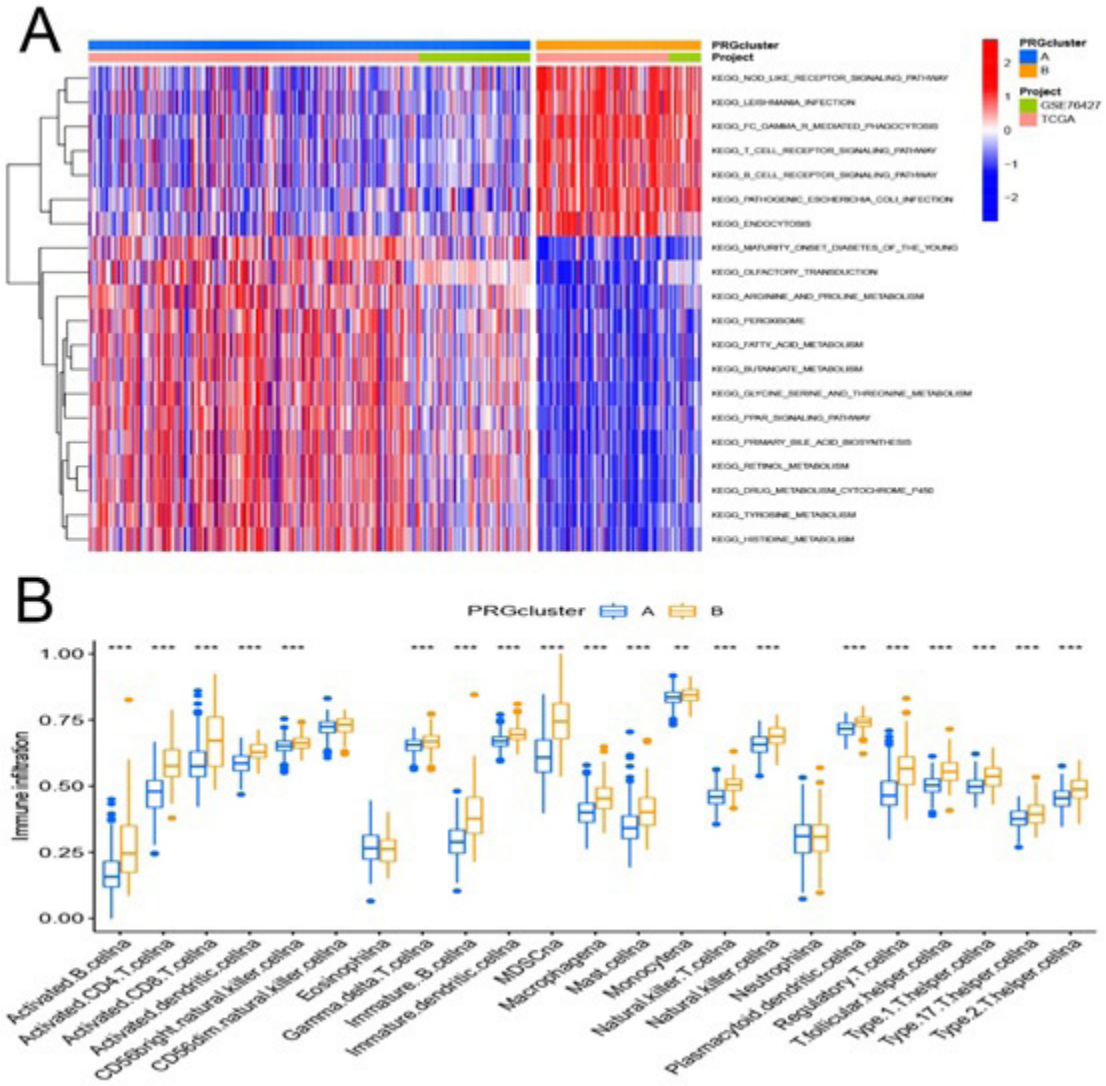

Figure 3: Correlation of tumor immune cell microenvironment with two HCC subtypes. (A) GSVA analysis of biological pathways between two different isoforms, where red and blue represent high- and low-expressing pathways, respectively. (B) Abundance of 23 infiltrating immune cell types in the two HCC subtypes. GSVA, Gene Set Variation Analysis;

4.4. Isotyping of differentially expressed genes

To explore the underlying biological behavior of each pyroptosis type, we identified 2724 pyroptosis type-related DEGs using the "VennDiagram" and "limma" packages in R studio software (Figure 4A), and performed GO and KEGG enrichment analysis. In Figure 4B, GO analysis indicated that the differential genes associated with these pyroptotic subtypes were significantly enriched in immune-related biological processes. In Figure 4C, KEGG enrichment analysis showed enrichment in immune- and cancer-related pathways such as Cytokine−cytokine receptor interaction. These results suggest that pyroptosis plays an important role in the immune regulation of the tumor microenvironment. Then we used the "survival" and "limma" packages in R studio software to analyze the differential genes to find the differential genes related to prognosis. To further verify this regulatory mechanism, we then performed differential genotyping, using a consensus clustering algorithm to classify patients into 3 genomic subtypes based on prognostic genes, genotype A, genotype B, and genotype C (Figure 4D). Then we performed genotyping survival analysis using the "survival" and "survminer" packages in R studio software. The Kaplan-Meier curve showed a significant difference in survival among the three types, with type B having the best prognosis while type C had the worst prognosis (Figure 5A). At the same time, it can be seen in Figure 5B that type C generally presents a high expression state in age, gender and tumor status. Figure 5C followed by differential analysis of genotyped pyroptosis genes, we found that pyroptosis-related genes generally had significant differences among the 3 subtypes.

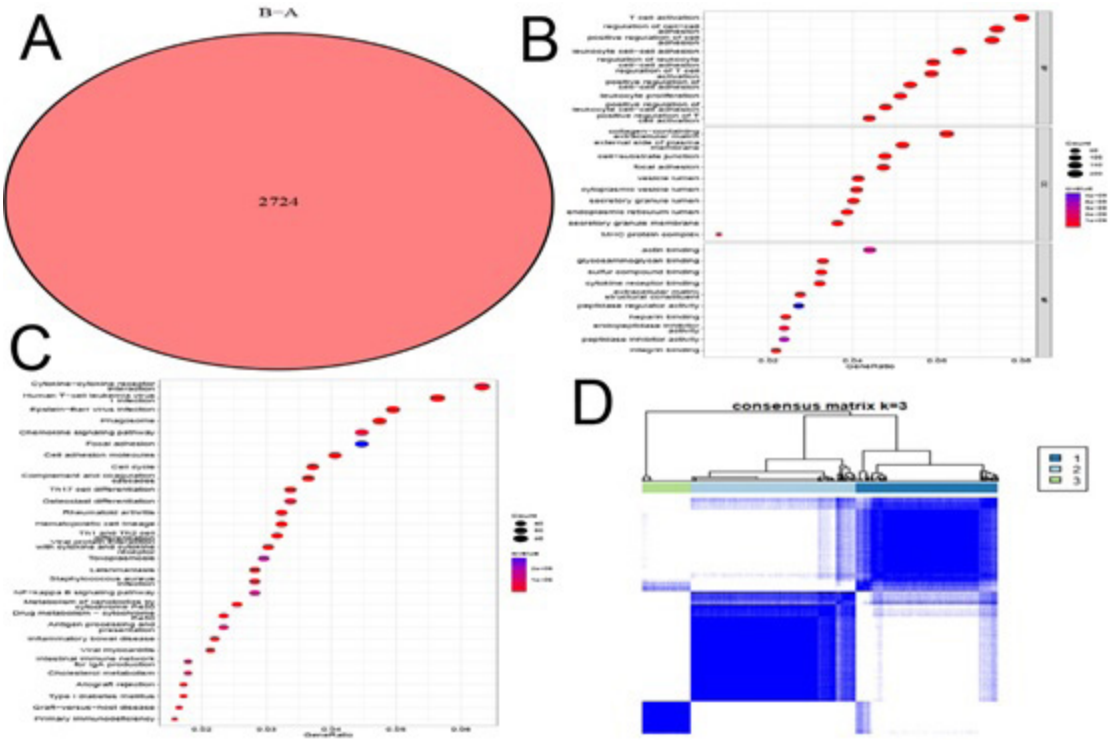

Figure 4: DEG-based genotyping. (A) The resulting differential genes. (B, C) GO and KEGG enrichment analysis of DEGs in two pyroptotic subtypes. (D) Consensus matrix heatmap defining three clusters (k = 3) and their associated regions. DEGs, differentially expressed genes; GO, Gene Ontology; KEGG, Kyoto Encyclopedia of Genes and Genomes;

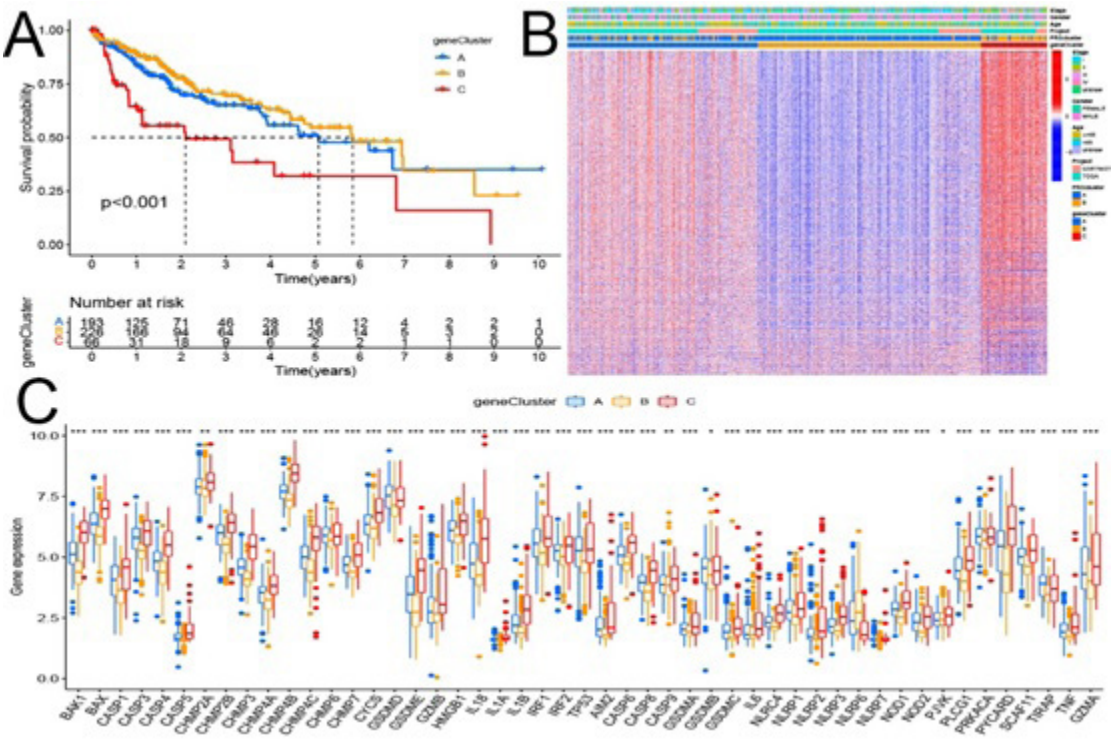

Figure 5: DEG-based genotyping. (A) Kaplan-Meier curves of survival for the two genotypes (log-rank test, p < .001). (B) Relationship between clinical features and the two genotypes. (C) Differences in the expression of 52 PRGs between the two genotypes.

4.5. Constructing a pyroptosis-related prognosis

The construction of the prognostic model is based on the expression of pyroptotic genes in different subtypes. All HCC patients were randomly divided into a train group (n=243) and a test group (n=242) at a ratio of 1:1, and Lasso regression and COX model were constructed based on the prognostic genes associated with pyroptosis (Figure 6A). According to the results of multivariate Cox regression analysis, the formula of the prognostic model is as follows: Risk Score = (-2.0158* MEI1 expression) + (0.4515* FHL3 expression) + (0.4732* DYNLT1 expression) + (0.3184* VRK2 expression) + (0.6452* TRIM21 expression) + (-0.4061* KLF2 expression) + (-0.1471* PLGLA expression) + (0.1561* GAGE2A expression) + (0.2109* SLC1A7 expression) + (-0.0986* TRIM55 expression). Based on the median risk score, the train and test groups were divided into low-risk (PRG_score < median) and high-risk (PRG_score > median) groups, respectively.

In Figure 6B, the patient distribution for two pyroptotic subtypes, three genetic subtypes, and two prognostic model groups is shown. First, the samples were divided into two subtypes (subtype A and subtype B) according to the expression of pyroptotic cell genes, and then the two subtypes were analyzed for differential genes and related differential genes were found. The expression levels of differentially expressed genes were classified to obtain subtype A, subtype B and subtype C. Finally, survival analysis was performed on the differential genes, and the differential genes related to prognosis were found to construct a prognostic model (high-risk group and low-risk group). We then performed a differential analysis of risk scores and found significant differences in risk scores between pyroptotic genotypes. Subtype B had a higher risk score than subtype A (Figure 6C). Figure 6D shows that in geneCluster, there are also significant differences between the three subtypes, with the B subtype having the lowest risk score and the C subtype having the highest risk score. Patients were divided into low-risk (PRG_score <median) and high-risk (PRG_score >median) groups according to the median risk score. In Figure 6E, we then performed a differential analysis of risk, it can be seen that most genes have significant differences in the expression of high and low risk groups and except for these genes (GZMB, IL18, IL6 and GZMA), other cell pyroptosis All related genes were highly expressed in the high-risk group. In Figure 7, Kaplan-Meier survival curves show that overall survival was significantly improved in low-risk patients compared with high-risk patients. Finally, we plotted the risk curve (Figure 8B1-2), and as the risk score increased, so did the number of patients who died. At the same time, six high-risk genes, FHL3, DYNLT1, VRK2, TRIM21, GAGE2A, and SLC1A7, can be obtained. The expression of these genes increases with the increase of the risk score; the four genes MEI1, KLF2, PLGLA, and TRIM55 increase with the risk of an increase in the score decreases its expression.

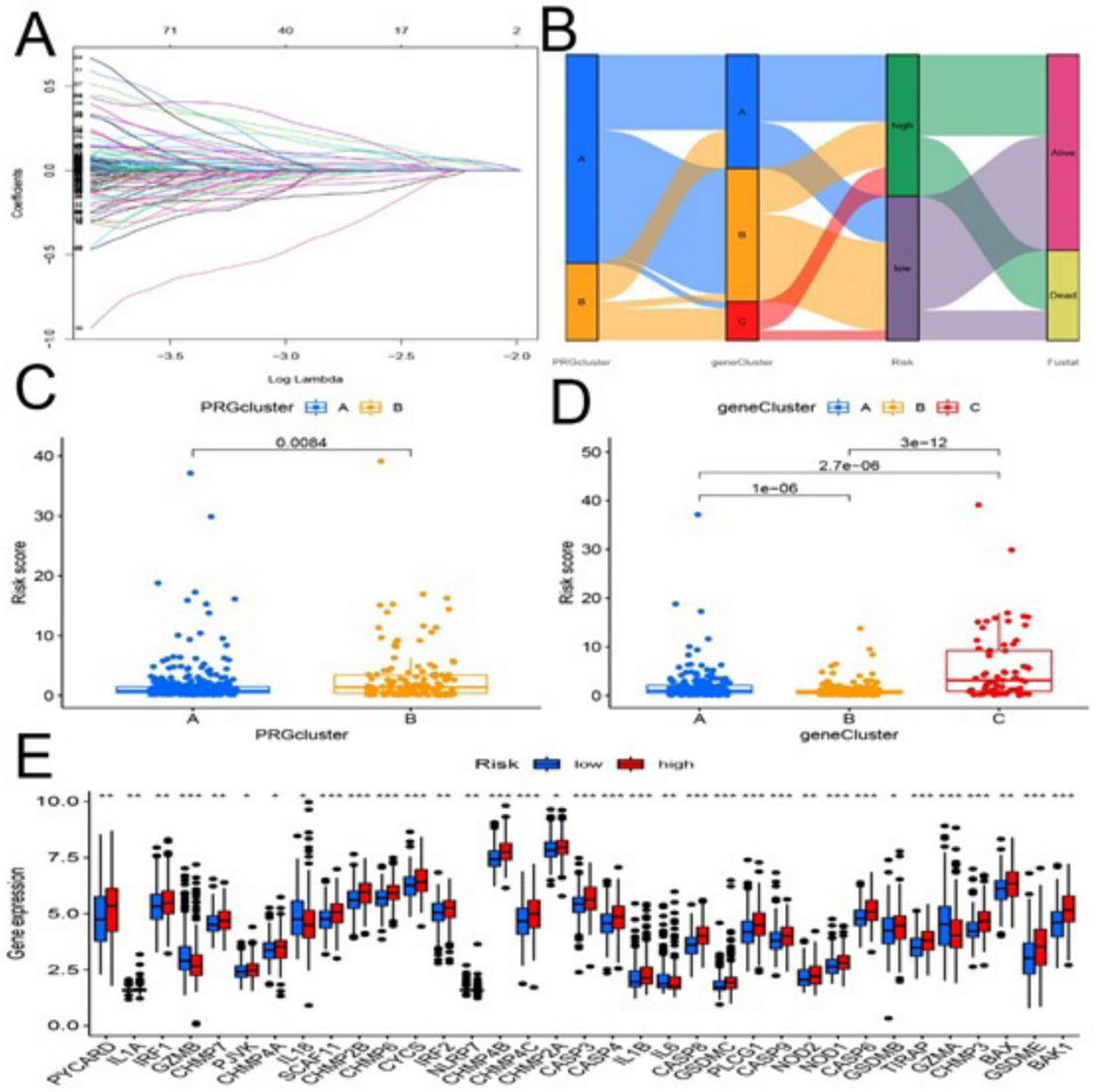

Figure 6: Construction of a prognostic model in the training set. (A) Model for lasso regression. (B) Sankey diagram of the distribution of subtypes in groups with different risk and survival outcomes. (C) Differences in risk scores between genotypes. (D) Differences in risk scores between pyroptosis subtypes. (E) Differential analysis of pyroptosis genes in high and low risk groups

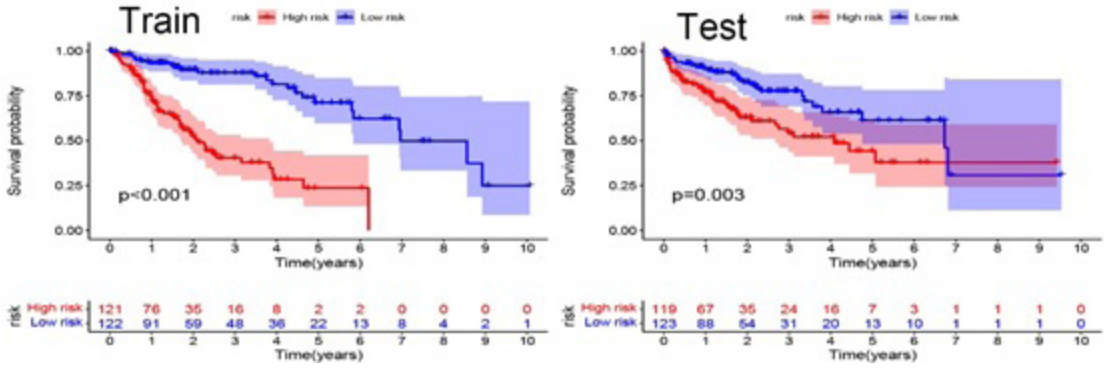

Figure 7: Kaplan-Meier analysis of survival between two groups

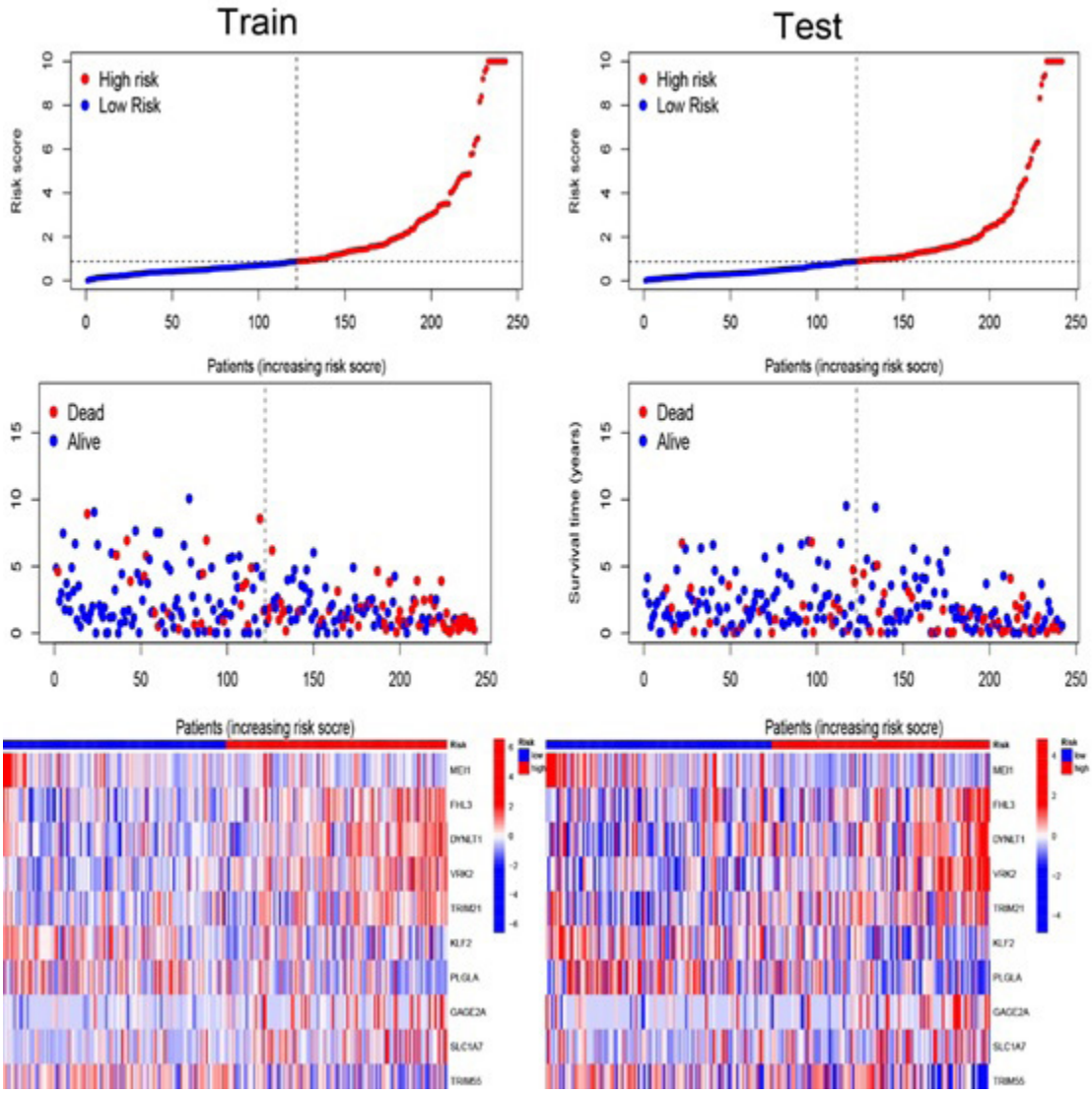

Figure 8: Risk curves between the two groups. In the three graphs, the risk gradually increases from left to right. Consists of Risk Score, Survival Time, and Risk Heatmap.

4.6. Correlation analysis of immune infiltration and tumor microenvironment

We performed the CIBERSORT algorithm to assess the association between genes involved in model construction and immune cell infiltration content. As shown in the scatter plots (Figures 9A and 9B), patient risk scores were positively correlated with Macrophages M2 and negatively correlated with T cells CD8. Then the differential analysis of the tumor microenvironment was performed (Figures 9C). StromalScore, ImmuneScore, and ESTIMATEScore were significantly different in the high and low risk groups, and the StromalScore, ImmuneScore, and ESTIMATEScore were higher in the low risk group. Finally, we also evaluated the relationship between 10 genes in the proposed model and immune cell abundance. In Figure 9D, we observed that most immune cells were significantly associated with 2 genes (DYNLT1, MEI1).

4.7. Correlation analysis of tumor mutation and drug sensitivity

There is increasing evidence that patients with high TMB may benefit more from immunotherapy due to their higher numbers of neoantigens [19-21]. In the correlation scatterplot (Figure 10A), the risk scores of patients in the three subtypes of genotyping were positively correlated with tumor mutational burden. Next, we analyzed the changes in the distribution of somatic mutations between the high and low risk groups. The top five mutated genes in the high and low risk groups were TP53, CTNNB1, TTN, MUC16, and ALB, respectively (Figure 10B and 10C). Compared with low-risk patients, CTNNB1, TTN, MUC16, and ALB mutation frequencies were significantly higher in high-risk patients, however, the exact opposite was observed with regard to TP53 mutation levels. Finally, we selected chemotherapeutic drugs currently commonly used to treat tumors to assess the sensitivity of low-risk and high-risk populations to these drugs. In Figure 11, we looked for drug names with significant differences in drug sensitivity between high and low risk groups. The IC50 values of Sorafenib, Doxorubicin, Embelin, Epothilone.B, Gemcitabine, JNK.Inhibitor.VIII, Obatoclax.Mesylate, Shikonin, Thapsigargin were significantly lower in high-risk patients. IC50 values were significantly higher for Temsirolimus, Roscovitine and Lenalidomide.

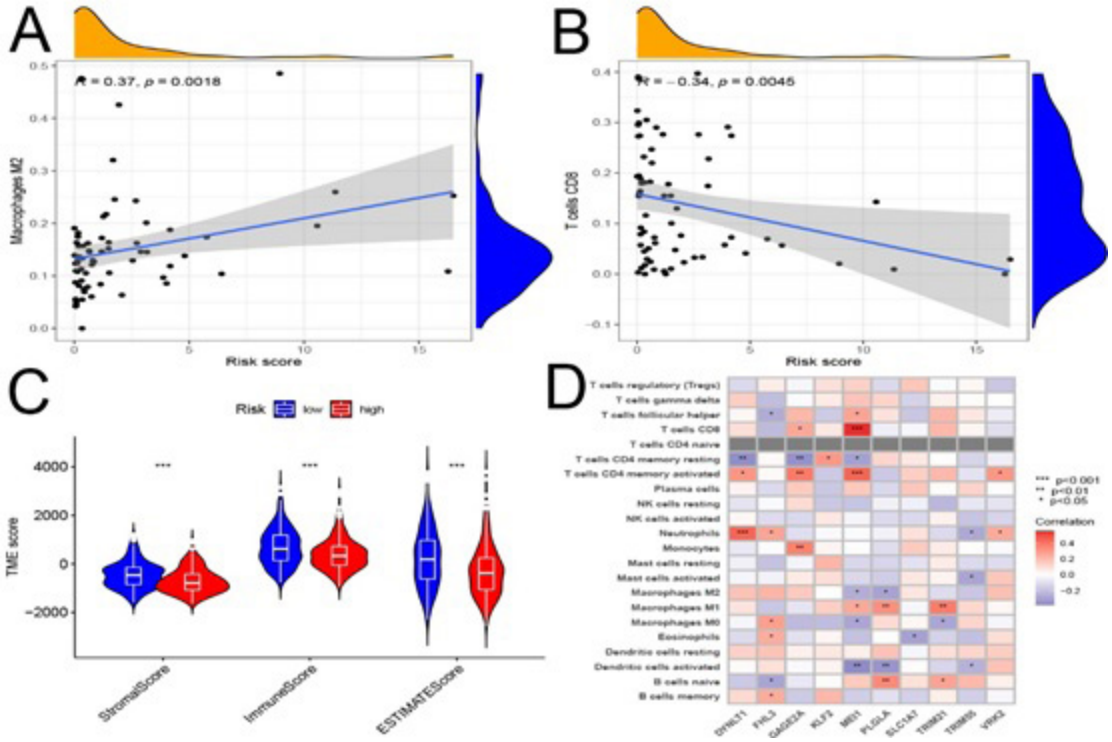

Figure 9: TME and checkpoint assessment between the two groups. (A) Correlation between risk score and immune cell type. (B) Correlations between risk scores and immune and stromal scores. (D) Correlation between immune cell abundance and ten genes in the proposed model. TME, tumor microenvironment

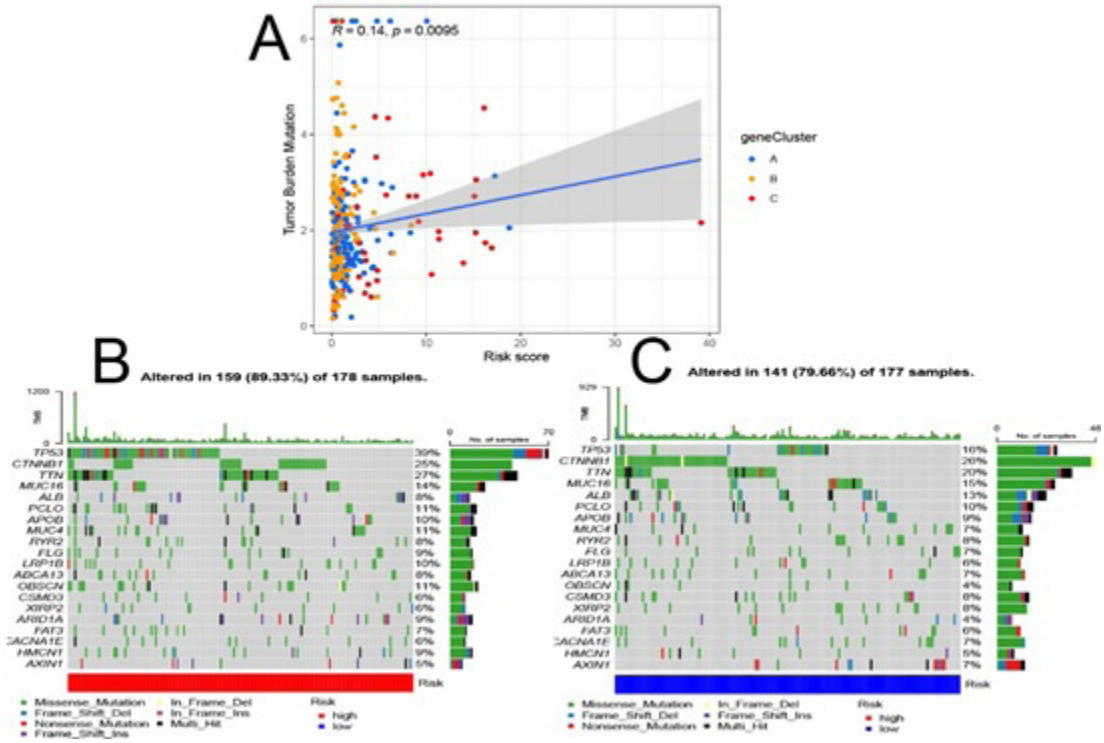

Figure 10: Analysis of risk scores in HCC. (A) Spearman correlation analysis of risk score and TMB. (B, C) Waterfall plots of somatic mutation signatures established with high and low risk scores. Each column represents an individual patient. The bar graph above shows TMB, and the numbers on the right represent the mutation frequency for each gene. The bar graph on the right shows the proportion of each variant type. TMB, tumor mutational burden

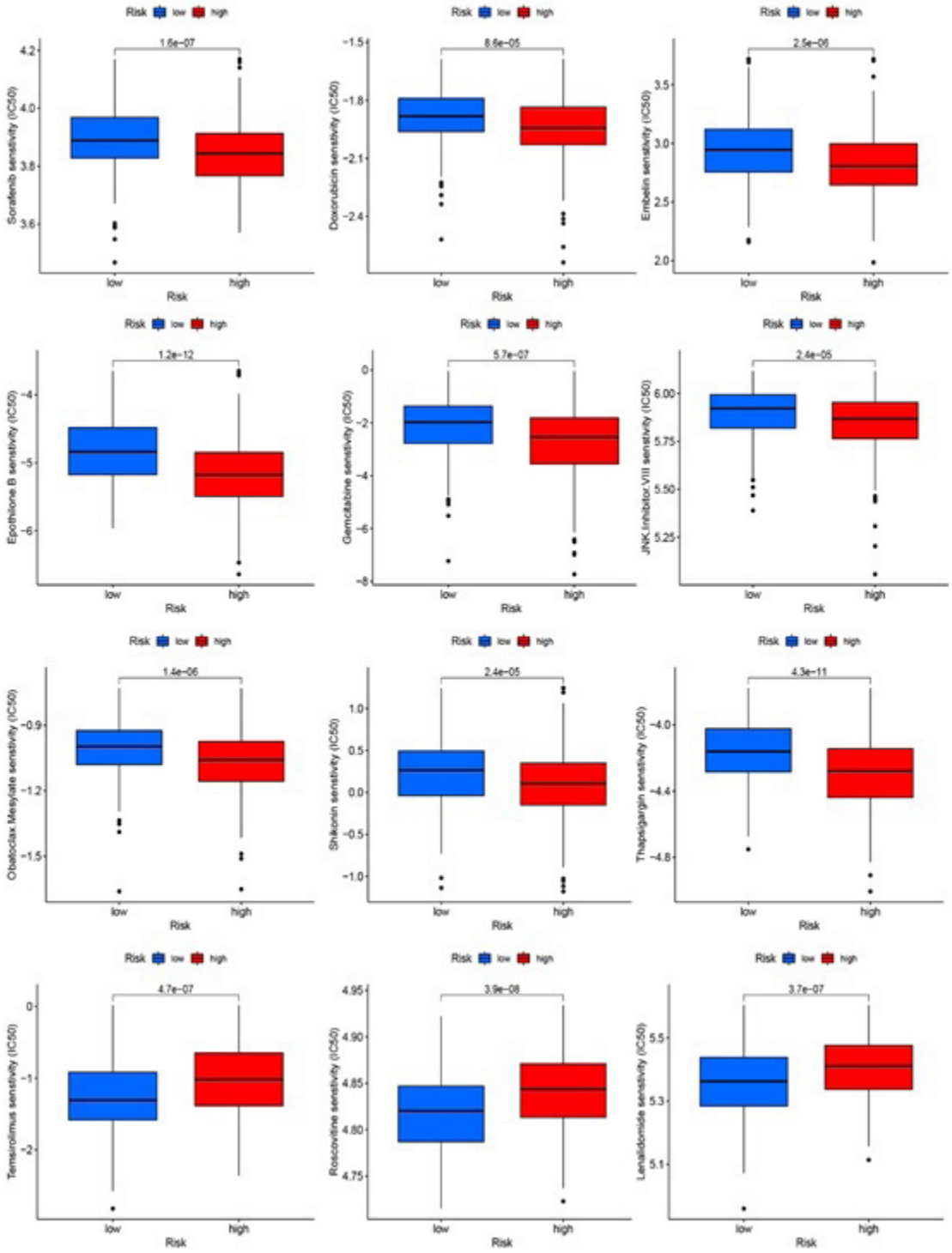

Figure 11: Relationship between risk score and chemosensitivity.

4.8. Nomogram to predict patient survival

Considering the inconvenient clinical application of the risk score in predicting survival of HCC patients, a nomogram including the risk score and clinical parameters was established to predict the survival rate of 1, 3, and 5 (Figure 12A). It can also be seen in Figure 12B that the model we constructed has high accuracy in predicting the 1, 3, and 5-year survival of patients. Predictors included risk score and patient stage. The results of our AUC experiments on the nomogram model (Figure 12C1-3) show that in the training set and test set, the accuracy of patient survival at 1, 3, and 5 years is high.

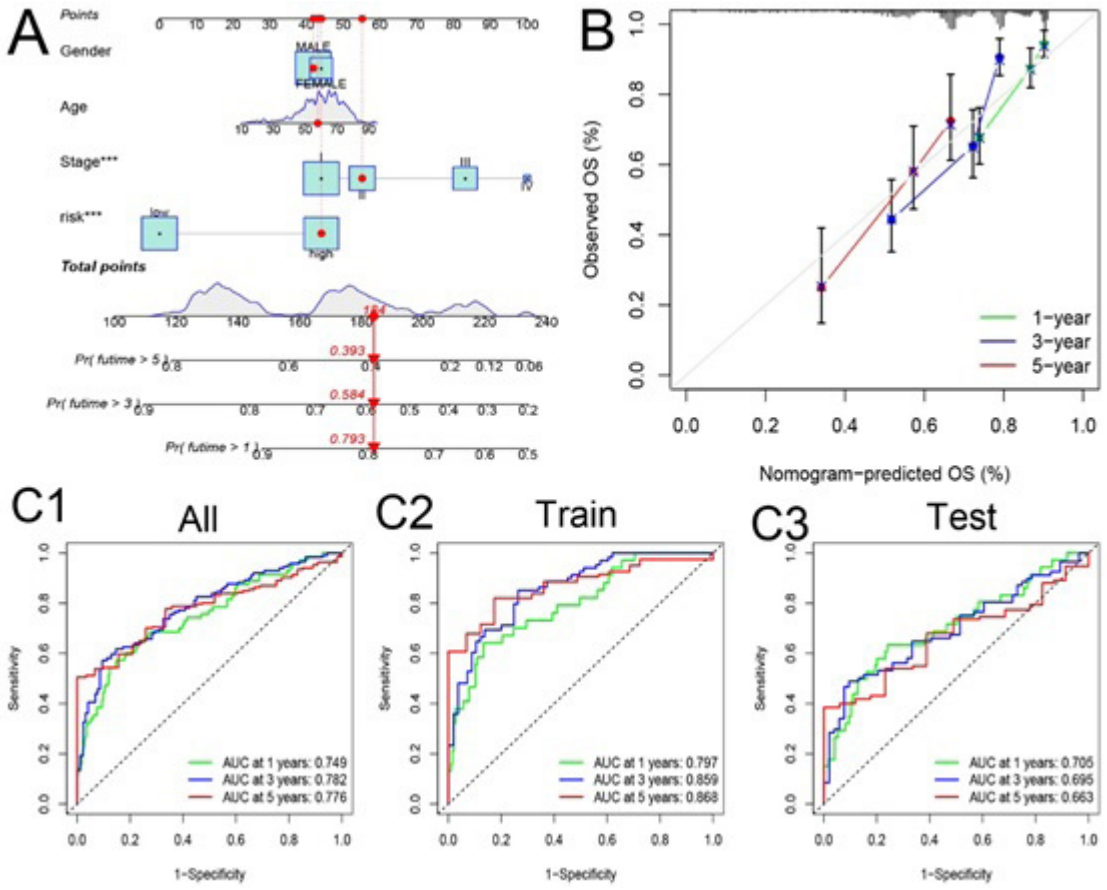

Figure 12: Construction and validation of the nomogram. (A) Nomogram used to predict 1-, 3-, and 5-year survival of CRC patients in the training set. (B) Calibration curves for nomograms used to predict and test 1-, 3-, and 5-year survival in the GSE 76427 set. (C1-3) ROC curves used to predict the 1-, 3-, and 5-year ROC curves in the GSE 76427 set.

5. Discuss

Most of the previous studies only evaluated the role of one or a few pyroptosis-related genes in anti-tumor, however, the anti-tumor effect is carried out by many genes in a highly coordinated manner [22]. The antitumor effect mediated by the combined action of multiple PRGs has not yet been fully elucidated. The results of this study reveal the overall alteration of PRGs in HCC at the transcriptional and genetic levels. We identified two distinct molecular subtypes based on 52 PRGs. Subtype A was found to have a higher survival rate than subtype B during the first 5 years. Comparing the clinical features of the two subtypes revealed significant differences in PRG expression and clinical features, most of the pyroptosis-related genes were generally highly expressed in subtype A in age, gender, and tumor status. There are also significant differences between the two subtypes in the tumor microenvironment, including NOD_LIKE_RECEPTOR_SIGNALING_PATHWAY, LEISHMANIA_INFECTION, FC_GAMMA_R_MEDIATED_PHAGOCYTOSIS, T_CELL_RECEPTOR_SIGNALING_PATHWAY, B_CELL_RECEPTOR_SIGNALING_PATHWAY and other pathways. Most of the two subtypes also had significant differences in immune cell infiltration, and the infiltration of Eosinophilna in subtype A was significantly higher than that in subtype B. In Activated.CD4.T.cellna, Gamma.delta.T.cellna, Immature..B.cellna, Mast.cellna, Natural.killer.T.cellna, T.follicular.helper.cellna, B subtype is obvious higher than subtype A. Meanwhile, we identified three genotypes based on the DEG between the two pyroptotic subtypes.

Our findings suggest that PRG may serve as a predictor for assessing clinical outcomes and immunotherapy response in HCC patients. Therefore, we constructed a stable and effective prognostic model. Through our validation, patients showed significantly different clinicopathological features, prognosis, TME, MSI, and drug sensitivity in low-risk and high-risk groups. Except for these genes (GZMB, IL18, IL6 and GZMA), other pyroptosis-related genes were highly expressed in the high-risk group. The high-risk group also had poorer survival and prognosis. Finally, we also obtained 6 high-risk genes, FHL3, DYNLT1, VRK2, TRIM21, GAGE2A, and SLC1A7, and the expression of these genes increased with the increase of risk score; four low-risk genes, MEI1, KLF2, PLGLA, and TRIM55 Its expression decreased with increasing risk score. In the differential analysis of the tumor microenvironment, we found that the StromalScore, ImmuneScore, and ESTIMATEScore were significantly different in the high- and low-risk groups, and the StromalScore, ImmuneScore, and ESTIMATEScore were higher in the low-risk group. Published studies have indicated that immunoscore-based assessment of prognostic value can provide additional evidence for the biological basis of immunotherapy [23, 24]. In the study of tumor mutation burden,

we analyzed the changes in the distribution of somatic mutations between high and low risk groups. The top five mutated genes in the high and low risk groups were TP53, CTNNB1, TTN, MUC16, and ALB, respectively. Compared with low-risk patients, CTNNB1, TTN, MUC16, and ALB mutation frequencies were significantly higher in high-risk patients, however, the exact opposite was observed with regard to the mutation levels of TP53. Previous studies have reported a negative role of TP53 mutations in tumor immunotherapy response and are associated with immunogenicity and tumor immune microenvironment characteristics [25, 26]. Pyroptosis induces local inflammation by attracting inflammatory cells, thereby alleviating immunosuppression and inducing an immune response in the TME. Under normal conditions, TME plays a role in homeostasis for tumor stroma maintenance and acts as a barrier to tumorigenesis. But when cells become cancerous, the surrounding stroma also changes to support tumor progression [14]. It can be seen that the tumor microenvironment plays a key role in the occurrence and development of liver cancer. GSVA enrichment analysis showed that subtype B was significantly enriched in several immune fully activated pathways, including NOD_LIKE_RECEPTOR_SIGNALING_PATHWAY, T_CELL_RECEPTOR_SIGNALING_PATHWAY and B_CELL_RECEPTOR_SIGNALING_PATHWAY. T and B cell receptor signaling pathways are significantly enriched in subtype B, and subtype B shows better survival and prognosis than subtype A, suggesting that T and B cells are involved in the immune defense of liver cancer play an important role. This is similar to previous findings that T and B cells play a crucial role in the immune defense of HCC [27]. Finally, by integrating prognostic models and tumor staging, we established quantitative nomograms that further improved performance and facilitated the use of prognostic models. This prognostic model can be used for the prognosis stratification of liver cancer patients, which is helpful to better understand the molecular mechanism of liver cancer, and may provide new directions and ideas for future targeted immunotherapy.

In this study, a pattern of pyroptosis characterized by immune activation (subtype B) was associated with high risk, and the infiltrating immune cells in subtype B were Macrophages M2. Tumor-associated macrophages are divided into two major phenotypes: M1 macrophages (suppressing cancer progression) and M2 macrophages (promoting cancer progression) [28]. In the present study, the high-risk group had higher levels of M2 in macrophages, which are immunosuppressive and contribute to matrix remodeling to favor tumor growth. Previous studies have shown that loss of M2 polarization is associated with reduced long-term inflammation and regeneration following liver injury [29]. This may provide new ideas for future immunotherapy. In the differential analysis of the tumor microenvironment, we found that the StromalScore, ImmuneScore, and ESTIMATEScore were significantly different in the high- and low-risk groups, and these scores were higher in the low-risk group. Finally, we also evaluated the relationship between 10 genes in the proposed model and immune cell abundance and found that most immune cells were significantly associated with these 2 genes (DYNLT1, MEI1). Further research on these two genes may provide new directions for tumor immunotherapy. Finally, we selected the chemotherapy drugs currently commonly used in the treatment of tumors and found that in high-risk patients, the IC50 of Sorafenib, Doxorubicin, Embelin, Epothilone.B, Etoposide, Gemcitabine, JNK.Inhibitor.VIII, Obatoclax.Mesylate, Shikonin, Thapsigargin value is significantly lower. Among the above sensitive drugs, only Sorafenib [30] has a long history of clinical application. Research on other drugs may be able to find more new immune drugs for the treatment of liver cancer. IC50 values were significantly higher for Temsirolimus, Roscovitine and Lenalidomide. The discovery of these drugs may provide new ideas and directions for future immunotherapy of liver cancer. This study has several limitations. First, all analyses were performed only on data from public databases. Therefore, large-scale prospective studies and additional in vivo and in vitro experimental studies are required to confirm our findings. Furthermore, in most datasets, data on some important clinical variables such as surgery, neoadjuvant chemotherapy, and chemoradiotherapy were not available for analysis, which may have affected the immune response and prognosis of pyroptotic status.

7. Conclusion

Our comprehensive analysis of pyroptotic genes reveals their broad regulatory mechanisms that affect tumor-immunity-tumor microenvironment and prognosis. We also identified an important role for PRG in targeted therapy and immunotherapy. These findings highlight the important clinical significance of PRG and may provide new ideas for guiding future personalized immunotherapy strategies for HCC patients.

References

1. Garcia-Pras E, Fernandez-Iglesias A, Gracia-Sancho J, Perez-Del-Pulgar S. Cell Death in Hepatocellular Carcinoma: Pathogenesis and Therapeutic Opportunities. Cancers (Basel). 2021; 14:
2. Nafie MS, Khodair AI, Hassan HAY, El-Fadeal NMA, Bogari HA, Elhady SS, et al. Evaluation of 2-Thioxoimadazolidin-4-one Derivatives as Potent Anti-Cancer Agents through Apoptosis Induction and Antioxidant Activation: In Vitro and In Vivo Approaches. Molecules. 2021; 27:
3. Niu Z, Xu Y, Li Y, Chen Y, Han Y. Construction and validation of a novel pyroptosis-related signature to predict prognosis in patients with cutaneous melanoma. Math Biosci Eng. 2022; 19: 688-706.
4. Liu X, Ding S, Liu P. The Roles of Gasdermin D in Coronavirus Infection and Evasion. Front Microbiol. 2021; 12: 784009.
5. Zhang YF, Zhou L, Mao HQ, Yang FH, Chen Z, Zhang L. Mitochondrial DNA leakage exacerbates odontoblast inflammation through gasdermin D-mediated pyroptosis. Cell Death Discov. 2021; 7: 381.
6. Song Z, Gong Q, Guo J. Pyroptosis: Mechanisms and Links with Fibrosis. Cells. 2021; 10.
7. Chu Q, Jiang Y, Zhang W, Xu C, Du W, Tuguzbaeva G, et al. Pyroptosis is involved in the pathogenesis of human hepatocellular carcinoma. Oncotarget. 2016; 7(51): 84658-84665.

8. Wree A, Eguchi A, McGeough MD, Pena CA, Johnson CD, Canbay A, et al. NLRP3 inflammasome activation results in hepatocyte pyroptosis, liver inflammation, and fibrosis in mice. Hepatology. 2014; 59: 898-910.
9. Yan W, Chang Y, Liang X, Cardinal JS, Huang H, Thorne SH, et al. High-mobility group box 1 activates caspase-1 and promotes hepatocellular carcinoma invasiveness and metastases. Hepatology. 2012; 55: 1863-75.
10. Teng JF, Mei QB, Zhou XG, Tang Y, Xiong R, Qiu WQ, et al. Polyphyllin VI Induces Caspase-1-Mediated Pyroptosis via the Induction of ROS/NF-kappaB/NLRP3/GSDMD Signal Axis in Non-Small Cell Lung Cancer. Cancers (Basel). 2020; 12.
11. Li H, Zhao XK, Cheng YJ, Zhang Q, Wu J, Lu S, et al. Gasdermin D-mediated hepatocyte pyroptosis expands inflammatory responses that aggravate acute liver failure by upregulating monocyte chemotactic protein 1/CC chemokine receptor-2 to recruit macrophages. World J Gastroenterol. 2019; 25(44): 6527-40.
12. Xiang R, Ge Y, Song W, Ren J, Kong C, Fu T. Pyroptosis Patterns Characterized by Distinct Tumor Microenvironment Infiltration Landscapes in Gastric Cancer. Genes (Basel). 2021; 12.
13. Tan Y, Chen Q, Li X, Zeng Z, Xiong W, Li G, et al. Pyroptosis: a new paradigm of cell death for fighting against cancer. J Exp Clin Cancer Res 2021; 40: 153.
14. Hinshaw DC, Shevde LA. The Tumor Microenvironment Innately Modulates Cancer Progression. Cancer Res. 2019; 79: 4557-66.
15. Chen F, Zhuang X, Lin L, Yu P, Wang Y, Shi Y, et al. New horizons in tumor microenvironment biology: challenges and opportunities. BMC Med. 2015; 13: 45.
16. Conesa A, Madrigal P, Tarazona S, Gomez-Cabrero D, Cervera A, McPherson A, et al. A survey of best practices for RNA-seq data analysis. Genome Biol. 2016; 17: 13.
17. Ye Y, Dai Q, Qi H. A novel defined pyroptosis-related gene signature for predicting the prognosis of ovarian cancer. Cell Death Discov. 2021; 7: 71.
18. Zhang Y, He R, Lei X, Mao L, Jiang P, Ni C, et al. A Novel Pyroptosis-Related Signature for Predicting Prognosis and Indicating Immune Microenvironment Features in Osteosarcoma. Front Genet. 2021; 12.
19. Burcher KM, Lantz JW, Gavrila E, Abreu A, Burcher JT, Faucheux AT, et al. Relationship between Tumor Mutational Burden, PD-L1, Patient Characteristics, and Response to Immune Checkpoint Inhibitors in Head and Neck Squamous Cell Carcinoma. Cancers (Basel). 2021; 13:
20. Kim H, Kim H, Kim R, Jo H, Kim HR, Hong J, et al. Tumor Mutational Burden as a Biomarker for Advanced Biliary Tract Cancer. Technol Cancer Res Treat. 2021; 20: 15330338211062324.
21. Snyder A, Makarov V, Merghoub T, Yuan J, Zaretsky JM, Desrichard A, et al. Genetic basis for clinical response to CTLA-4 blockade in melanoma. N Engl J Med. 2014; 371: 2189-99.
22. Tsuchiya K. Switching from Apoptosis to Pyroptosis: Gasdermin-Elicited Inflammation and Antitumor Immunity. Int J Mol Sci. 2021; 22.
23. Luo J, Xie Y, Zheng Y, Wang C, Qi F, Hu J et al. Comprehensive insights on pivotal prognostic signature involved in clear cell renal cell carcinoma microenvironment using the ESTIMATE algorithm. Cancer Med. 2020; 9: 4310-23.
24. Yang P, Chen W, Xu H, Yang J, Jiang J, Jiang Y, et al. Correlation of CCL8 expression with immune cell infiltration of skin cutaneous melanoma: potential as a prognostic indicator and therapeutic pathway. Cancer Cell Int. 2021; 21: 635.
25. Hu C, Zhao L, Liu W, Fan S, Liu J, Liu Y, et al. Genomic profiles and their associations with TMB, PD-L1 expression, and immune cell infiltration landscapes in synchronous multiple primary lung cancers. J Immunother Cancer. 2021; 9.
26. Zeidan AM, Boss IW, Beach CL, Copeland WB, Thompson EG, Fox BA, et al. A Randomized Phase 2 Trial of Azacitidine ± Durvalumab as First-line Therapy for Higher-Risk Myelodysplastic Syndromes. Blood Adv. 2021; 2021005487.
27. Zhou S, Fan C, Zeng Z, Young KH, Li Y. Clinical and Immunological Effects of p53-Targeting Vaccines. Front Cell Dev Biol. 2021; 9: 762796.
28. Pan Y, Yu Y, Wang X, Zhang T. Tumor-Associated Macrophages in Tumor Immunity. Front Immunol. 2020; 11: 583084.
29. Ortmayr G, Brunnthaler L, Pereyra D, Huber H, Santol J, Rumpf B, et al. Immunological Aspects of AXL/GAS-6 in the Context of Human Liver Regeneration. Hepatol Commun. 2021.
30. Reinkens T, Stalke A, Huge N, Vajen B, Eilers M, Schaffer V, et al. Ago-RIP Sequencing Identifies New MicroRNA-449a-5p Target Genes Increasing Sorafenib Efficacy in Hepatocellular Carcinoma. J Cancer. 2022; 13: 62-75.